Optimum Design of Hybrid Excavation Support System in Cohesionless Sand Using 2D and 3D Finite Element Analysis

Mohsen Khosravi

Department of Structural, Geotechnical and Building Engineering, Politecnico di Torino, Torino, Italy

Abstracts

The stability of deep excavations in cohesionless soils depends strongly on groundwater conditions and excavation geometry. Two-dimensional analyses, although widely applied, often fail to capture three-dimensional effects, leading to conservative designs. This study investigates an optimum hybrid support system; secant pile walls combined with prestressed tie-back anchors, through a three-stage methodology: A limit equilibrium analysis, followed by finite element simulations in PLAXIS 2D and PLAXIS 3D. A total of 81 scenarios were analyzed, considering soil density (loose, medium, stiff sands), surcharge loading (30 to 90 kN/m²), excavation depths (6 to 18 m), and groundwater levels. The results show that groundwater level is the dominant factor governing anchor demand, with normalized anchor consumption (β) increasing significantly as the water table rises. The hybrid system ensured stability across soil types by mobilizing pile resistance at depth and anchor efficiency against lateral displacement. Comparisons between 2D and 3D models revealed substantial differences: wall deformations predicted by 3D analyses were up to 62% smaller for 20 m wide excavations, 36% for 30 m, and 9% smaller for 50 m. Bending moments also decreased by as much as 62% in narrow excavations. The findings demonstrate that 3D modeling provides a more realistic representation of excavation performance. Moreover, the proposed β ratio further assists in evaluating anchor efficiency, helping prevent over-design while ensuring safety.

Keywords: 2D-3D Finite element analysis, Limit equilibrium method, Anchorage, Scant piles, Optimum design.

1. Introduction

The aim of the study is to compare the design, derived from analysis, the stability of an excavation in simple 2D finite element method and its 3D equivalent design. This study raised from the need of acquiring more accurate model, capable of representing the excavation condition closer to reality. An accurate representation will aid to identify the critical sections of the wall where the shear force and bending moments is at maximum and while also enabling the prediction wall displacement and associated soil movement. 3D dimensional modeling would also give better view of soil mechanism where simple 2D approximation can miss. The case history of CSC (soil-cement column) wall failure of Bangkok reservoir could have been prevented if 3D finite element modeling were implemented during design phase.[1]. It happens so often that due to irregularity of site geometry and complex installation detailing, 2D models cannot reproduce field displacements therefore 3D models are required. [2] Moreover, the accurate model could potentially reduce the construction cost by reducing the cost allocated for excavation stabilization by enabling better optimized plans, fewer contingency costs, more efficient and less wasteful designs. [3], [4], [5]

In this study, the stability of excavations in three types of cohesionless sand is evaluated

considering four key parameters: the surcharge load applied at the top of embankment, the underground water level (H), the excavation depth (D), and the excavation wall width (W). While excavations are 90° cuts, these scenarios are developed to ensure that the support system can maintain stability before, during, and after construction. The proposed stabilization strategy combines secant pile walls with tie-back anchors in a hybrid system designed to overcome the limitations inherent in each method used in isolation, particularly in soils prone to liquefaction, where single methods often fail to resist uplift pressures and lateral displacements. As demonstrated in an experimental study of double row micropile-anchor systems in deep fill soils, such composite designs are “feasible and exhibit good economic properties”, making them suitable system in weak soils.[6] Similarly, large-scale model tests have shown that prestressed anchors paired with piles significantly limits both horizontal displacement and bending stresses, thereby enhancing excavation stability.[7]. Moreover, post-earthquake investigations in liquefiable sand have demonstrated severe uplift and lateral spreading, with structures experiencing “lateral displacement of the anchored sheet-pile quay wall of approximately one meter with settlements of roughly 0.5 m to 0.6 m” during the 2007 Niigata Chuetsu-oki earthquake, highlighting the inadequacy of conventional systems in such conditions.[8]

Determining an optimal design to support excavation walls is essential, not only to guarantee safety but also to minimize construction costs by avoiding over-design. The Limit Equilibrium Method (LEM) is a widely adopted analytical approach due to its computational efficiency, and capability to provide an interpretable safety metric (Factor of Safety). When coupled with optimization routines, LEM, enables the exploration of design variables (reinforcement length, spacing, wall geometry), helps to identify configurations that achieve required safety factor at the lowest cost. For example, a study integrating Slide2 with a Python-based optimization workflow demonstrated that: “*the tool should produce a design that is not only valid and safe for the profile, but globally optimal as well*.” This highlights how automation helps ensure that all stages and scenarios satisfy safety targets while minimizing material usage.[9]

In construction projects involving deep excavation, stabilizing the excavation walls could take 1.5 % the entire construction budget ranging from 0.5 % to 2.5 % depending on project type and site complexity [10] or up to 40% in heavily engineered underground structures. [11]. This amount may increase if the engineer is uncertain about the soil behavior which can leads to overdesign. Moreover, the lack of comprehensive view during design phase will results in unrealistic outcomes. For instance, in 2D design approaches the width of excavation wall is not considered. As a result, the same design may be applied regardless of excavation width, whereas in reality deformation of excavation wall is influenced by this parameter.

To overcome these challenges and improve the reliability of the design, this study investigates the influence of excavation width on wall deformation by comparing 2D and 3D modeling approaches. By identifying the limitations of traditional methods, the goal is to develop a more accurate and cost-effective design strategy for excavation support systems. To this end, optimum design was identified for each scenario using limit equilibrium method. Optimum design with minimum factor of safety equal to 1.3 were then re-modelled using both 2D and 3D finite element modeling. GEOSTUDIO SLOPE/W was employed for limit equilibrium analysis while PLAXIS 2D and PLAXIS 3D were used for finite element simulations.

The results of this study showed that, on average, the horizontal deformation at the top

of the excavated wall in the 3D model with a 20 m width was 62% smaller than its 2D equivalent. For an excavation width of 30 m, the deformation was 36% smaller, and for a width of 50 m, it was 9% smaller compared to the 2D model.

2. Methodology

In this study, the performance of a hybrid support system; secant pile walls (Figure 1) reinforced with prestressed tie-back anchors, was investigated under varying soil conditions and excavation geometries. Three representative scenarios of cohesionless soils were selected to capture a realistic range of ground behavior: stiff sand, medium dense sand, and loose sand. The geotechnical properties adopted in the analysis are summarized in Table 1.

Table 1. Soil properties used in this study

Soil Type	Properties	Values
Stiff Sand	E_s	30000 KPa
	ν	0.35
	ϕ	35
	ɣ	20 KN/m3
Medium dense Sand	E_s	20000 KPa
	ν	0.35
	ϕ	30
	ɣ	18 KN/m3
Loose Sand	E_s	10000 KPa
	ν	0.35
	ϕ	25
	ɣ	16 KN/m3

In order to simplify the numerical modeling of secant pile walls, the concept of an equivalent diameter was adopted following the approach of Liao et al. [12]. The equivalent diameter allows the discontinuous, overlapping primary and secondary piles to be represented as a continuous wall element with uniform stiffness. An equivalent diameter of 1.8 m was selected for all models, corresponding to the geometry of the secant pile cross section. The secant piles were modeled as reinforced concrete elements with a compressive strength of $f'_c = 21\ MPa$. The stiffness parameters of the equivalent piles are reported in Table 3.

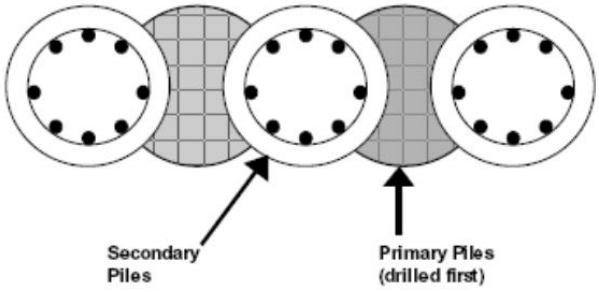

Figure 1. Schematic of a scant piles system

Table 2. Secant piles properties

Parameter		Values
EA		9.6 * 10^6 KN
EI		0.6*10^6 KN.m^2
Embedded Length	Stiff Sand	6 m
	Medium Sand	7.5 m
	Loose Sand	9.5 m

Three scenarios of excavation depth 6, 12 and 18 meters were considered. Embedded length or driving depth of the secant piles were determined using the Jumikis method [13] as a standalone system for factor of safety of at least 1.5, as reported in Table 2. The results then verified using Peck et al and Tschebotarioff, [14], [15] Designed embedded length fully satisfies the requirements for 6 and 12 meters. However, for 18 meters of excavation deemed unsafe indicating the need of a secondary support system or lengthening the depth of embedment. Also following the recommendations of Lees and Maleki [16],[17] the geometry of the numerical models was selected to be sufficiently large in order to minimize boundary effects on the excavation behavior. To achieve this, dimensions of the model (X_{max}, Y_{max}) were taken as approximately 3.5–3.75 times the excavation depth (Table 3), which is consistent with commonly adopted practice in deep excavation simulations. This ensures negligible boundary influence on wall deflections and ground settlements.

Table 3. Numerical model dimensions

Excavation depth (m)	X_{min} (m)	X_{max} (m)	Y_{min} (m)	Y_{max} (m)
6	0	21	0	15
12	0	42	0	30
18	0	63	0	45

Second system that integrated with the secant pile walls was the ground anchor system, also known as the tie back system. The anchor system or anchorage must be distinguished from the soil nailing method; which unlike soil nailing, this system is an active method, as the reinforcement is prestressed to apply tension which actively counteracts soil movement by pushing against the potential failure wedge. A typical ground anchor consists of two functional zones, namely the unbonded length and the bonded length (Figure 2). The unbonded length is the portion of the tendon (which could be steel bars or strands) that does not interact with the soil mass, allowing free elongation under prestressing. In contrast, the bonded length is the section in contact with the surrounding soil via cement grout, creating the anchorage zone. The bonded length essentially functions like a "stitching", anchoring the potential slide surface to the stable soil mass through grout-mediated shear transfer.

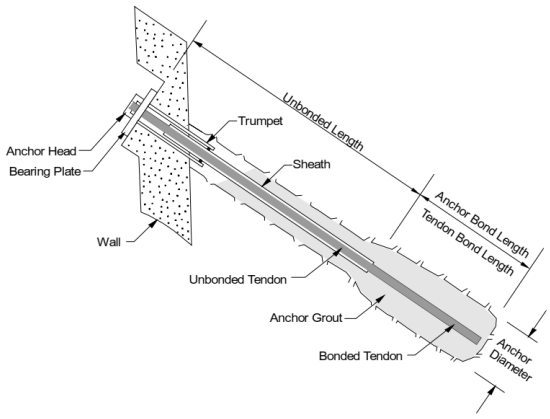

Figure 2. Components of a ground anchor.[18]

In this study, prestressed tendons were used as anchor reinforcement, specifically three-strand tendons (each with 15 mm diameter), ultimate tensile strength of 782.1 KN conforming to ASTM A416, Grade 270. The system diameter was assumed to be 0.1 m, with centralizers placed every 3 m along the length to ensure correct grouting. All anchors were installed at a 15° inclination relative to the horizontal, consistent with common excavation support practice.

According to the FHWA guidelines, both the ultimate tensile strength of the tendon system and the soil–grout bond capacity recommended to be reduced by safety factors of 2.0 and 1.5, respectively. or the selected configuration, the allowable design strand load equals to ($\frac{782.1}{2}$) ~ 391KN while the bond load capacity is given by:

$$\left(\frac{\tau b}{1.5}\right).\pi.d.L_b \qquad \textit{Equation 1}$$

Where τ_b is the soil–grout bonding stress in pressure grouted anchors given in Table 4, d=0.1 m is the system diameter, and L_b is the bond length. Therefore, ultimate allowable tensile capacity of a single anchor system is governed by the minimum of the two values.

Since the design tensile capacity of the strands is higher than the corresponding bond loads in all considered soil conditions, increasing the number of strands does not necessarily yield a higher anchor capacity. Therefore, the anchor design must be balanced between tendon strength and soil–grout interaction, ensuring efficiency and avoiding unnecessary material usage.

Table 4. Ultimate bond stress in pressure grouted anchors (straight shaft)

Cohesionless Soil	Stiff Sand	Medium Dense Sand	Loose Sand
Soil- Grout Bonding stress (Kpa)	350	250	150

To ensure the design is effective, scenarios were created based on the parameters

effecting the safety and design of the excavation. Namely surcharge load, q = 30, 60 and 90 KN/m^2 in length equal to depth of the excavation immediately at the top of the crest, Friction angle of the cohesionless soil (ϕ) and the depth of the excavation itself (H) and finally Water level H_w at the ground level (H_w=0), H_w=H/2 and H_w = H (bottom of the excavation). These variables yielded 81 different design scenarios. These scenarios at the first step modeled in GEOSTUDIO SLOPE/W a limit equilibrium software using bishop method with aim of finding the optimum design satisfying the safety factor of 1.3 for the critical slope surface. The secant piles were included in the model as active shear load cutting the critical slope surface as it cannot be modeled as a plate member in the software.[19] .Shear load 691.42 KN (Equation 2) was applied at tip toe of the critical slope surface where its location iteratively found on the wall where best represent the wall-slope surface interaction.

$$V = \frac{(\frac{1}{6}\sqrt{f'_c} * b_w * d) * 0.75}{1.5}$$

Equation 2

Where f'_c is the 28 days compressive strength of the reinforced concrete used in piles the b_w is the width of the wall which in 2D environment considered 1 meter, and d is the equivalent diameter of the secant piles. Figure 3 shows the optimum design modeled using limit equilibrium method.

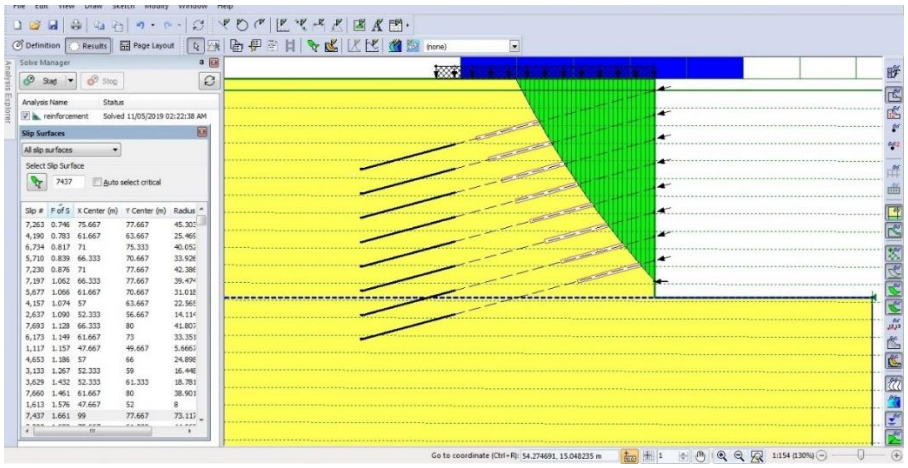

Figure 3. Finding optimum design using limit equilibrium method (GEOSTUDIO SLOPE/W)

The final design of each 81 scenario with exact same configuration in GEOSTUDIO SLOPE/W where modeled and set up for 2D finite element modeling in PLAXIS 2D software. The excavation phase introduced for every 2 meters of depth similar to real world practice (Figure 4).

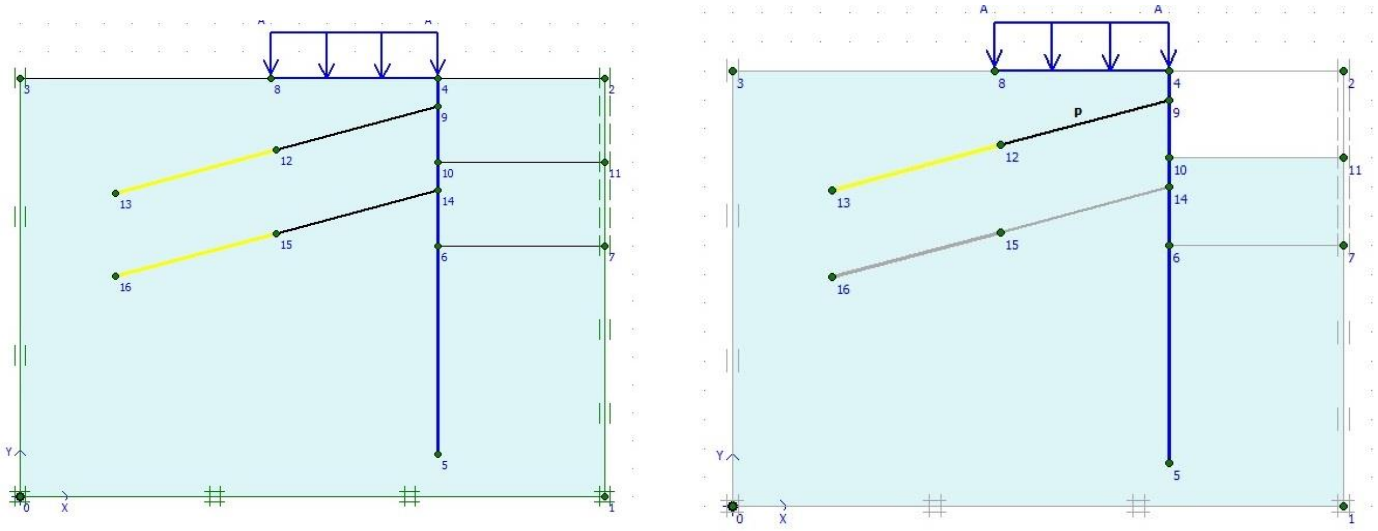

Figure 4. Finite element modeling using PLAXIS 2D (Excavation phase introduced for every 2 meters)

Same design configuration, were remodeled in 3D finite element environment using PLAXIS 3D with three different excavation widths of 20, 30 and 50 meters. Corner walls were also modeled with length equals to half of the excavation wall in question with same design configuration to take into consideration the corner effects. Figure 5 shows an example of a finite element model in PLAXIS 3D environment.

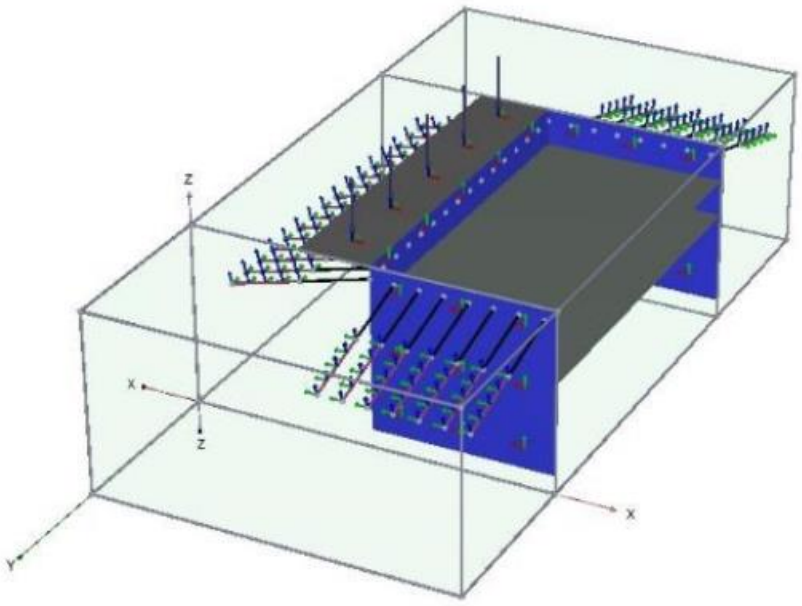

Figure 5. Finite element modeling using PLAXIS 3D

3. Results and Discussion

In order to normalize the rate of anchorage consumption in each design, a ratio β were introduced, which considers the length anchorage used in square meter of the excavated wall.

$$\beta = \frac{L}{A} \quad [\frac{1}{m}] \qquad \text{Equation 3}$$

Where L, is the length of the anchor, and A =(h_a*S_a) is the area of a smallest stabilized cell on the surface of the excavated wall (Figure 6). This ratio will aid in understanding if a suggested design is optimum or over design in related to the consumption of anchors.

The consumption rate of anchorage (β), were plotted against underground water level (Figure 7) for three considered excavation depths. These graph shows the mean value of anchorage consumption with standard deviations for surcharge loads 30 KN/m2 up to 90 KN/m2 and cohesionless soil with internal friction angle of 25 up to 35 degrees. Is evident, as the water level raises the anchorage consumption rate also increases

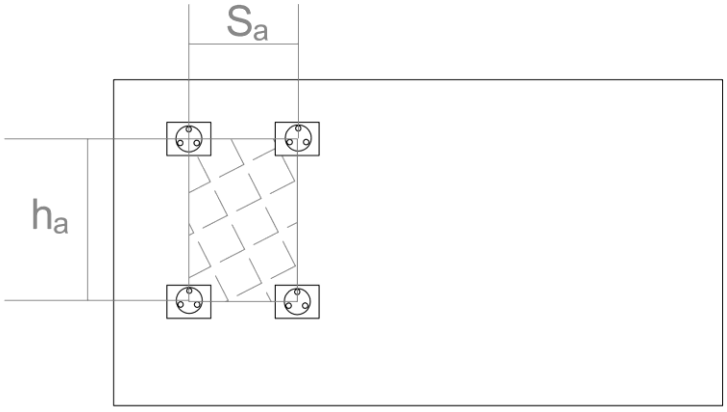

Figure 6. Smallest stabilized cell in the excavated wall. (Sa= Horizontal distance between two anchors, h_a= Vertical distance between two anchors)

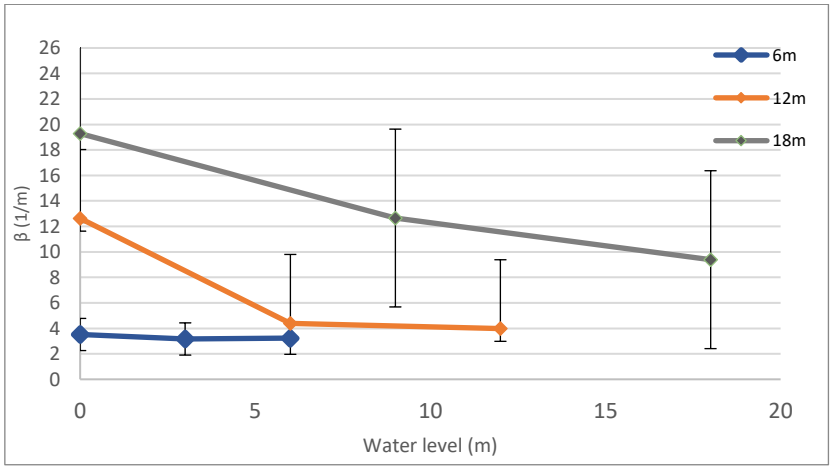

Figure 7.Anchorage consumption rate with respect to underground water level variation.

Cohesionless soils are generally considered in drained conditions. However, the influence of groundwater cannot be neglected in deep excavations. Hydrostatic pressure acts on the wall, independent of the reduction in shear strength already accounted for in effective

stress analysis. A comparative evaluation of surcharge-induced and hydrostatic pressures (Figure 8) illustrates the relative significance of these loads. For medium to deep excavations (12–18 m), hydrostatic pressure at groundwater level produces lateral loads on the order of 700–1500 KN/m per meter of wall, substantially greater than those induced by even heavy surface surcharges. Only in shallow cuts (~6 m) with high surcharge loads in loose sands the effects approach or exceed hydrostatic loads, which highlights the importance of groundwater control and considering drainage system coupled with excavation support in deep excavation design. The work of Kaiser and Hewitt, supports this theory, which demonstrated that groundwater flow influences not only lateral earth and water pressures on retaining structures but also the stability of the excavation floor with respect to piping and bulk heave.[20]

15 node triangular elements and 10 node tetrahedral elements were chosen to represent soil elements in PLAXIS 2D and PLAXIS 3D. Secant piles were represented using 6-nodes plate elements with only 5 degrees of freedom as they cannot sustain torsional moments. [21] Embedded beams, a special element in PLAXIS which based on the embedded beam approach by Sadek et al, [22] were used to describe the interaction of piles and anchors with surrounding soil.

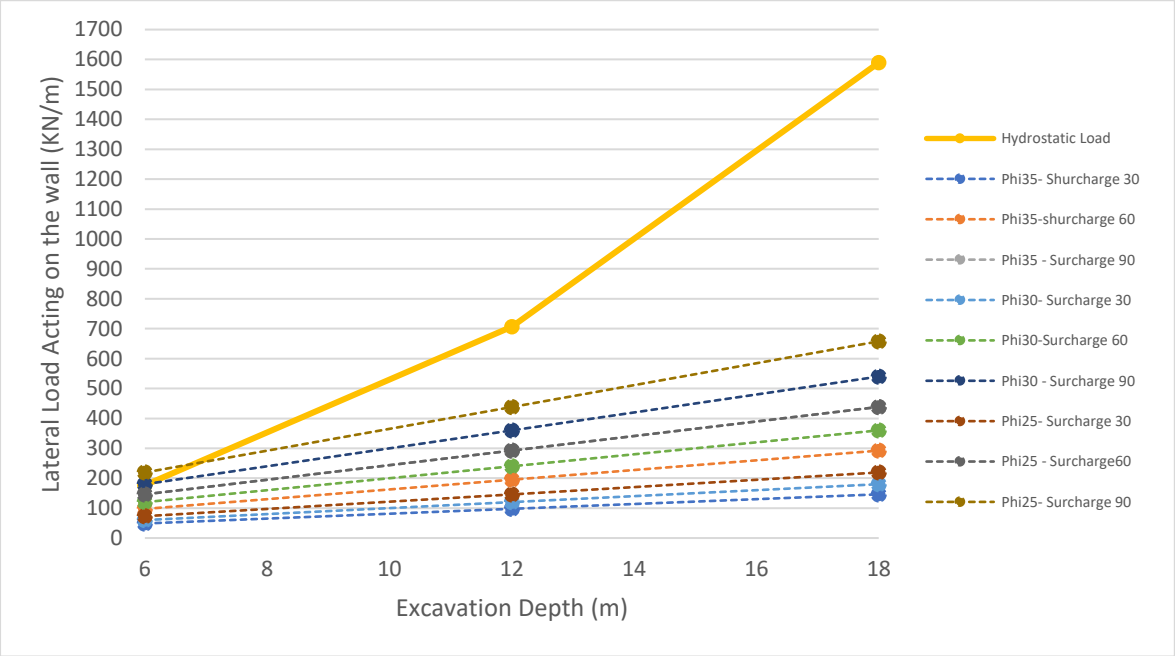

Figure 8. Lateral Loads acting on the excavated wall in considered scenarios

Finite element meshes generated using fine size elements in both 2D and 3D environment. 3D models created considering corner effects, with excavation widths of 20, 30 and 50 meters. In total 243 three dimensional models were developed for 81 considered scenarios. PLAXIS gives the ability to visualize the deformed mesh, the displacement and the acting forces of the entire system, including soil, walls and reinforcement either globally or discretely (Figure 9 and Figure 10). However, in this study, only the horizontal deformation and bending moment of the wall were investigated.

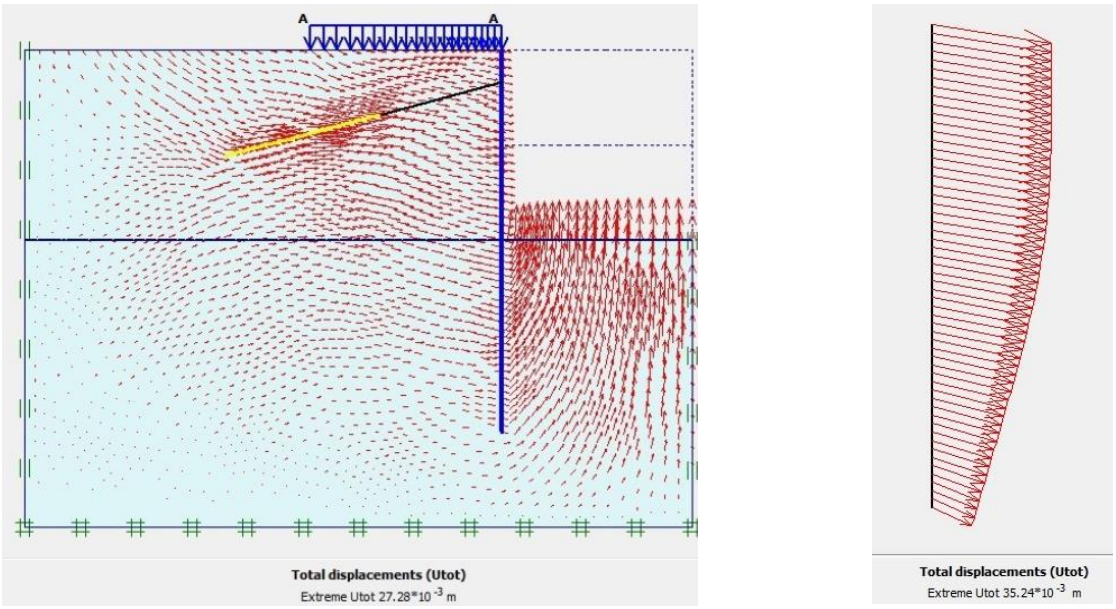

a) Total Displacements b) Total displacements of the wall

Figure 9. Results of the 2D finite element calculation

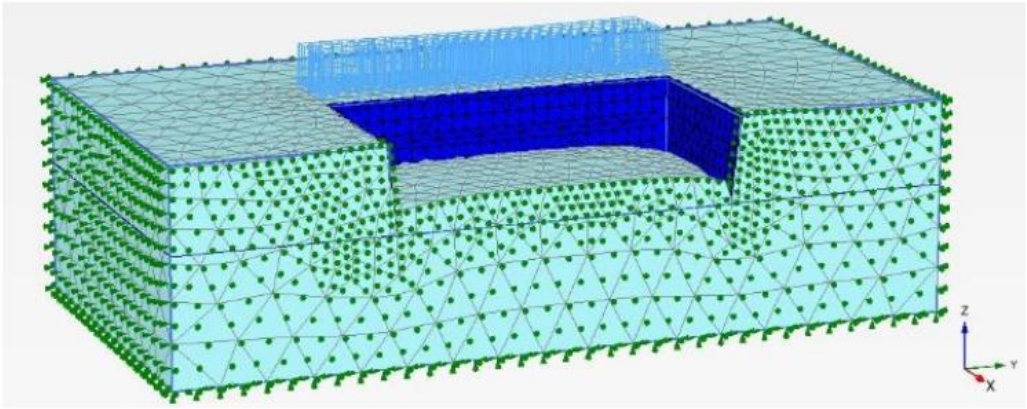

Figure 10. Deformed discretized model in PLAXIS 3D

The horizontal deformation of the wall is strongly influenced by hydrostatic conditions. In the following graphs, the “water level (m)” denotes the depth of the groundwater table below the ground surface (0 m = groundwater at ground level; larger values = deeper water table) (Figure 11 to Figure 13). When the groundwater table is near ground level, the wall is subjected to significant hydrostatic pressure which decreases soil stiffness and producing larger horizontal wall deformation. Conversely, drawdown of the water table reduces hydrostatic pressure and decreases pore pressure, thereby increasing effective stress and soil resistance; these changes manifest across all considered depths (6, 12 and 18 m). This behavior is consistent with established observations that groundwater boundary conditions strongly influence excavation response and settlement patterns.[20], [23] .

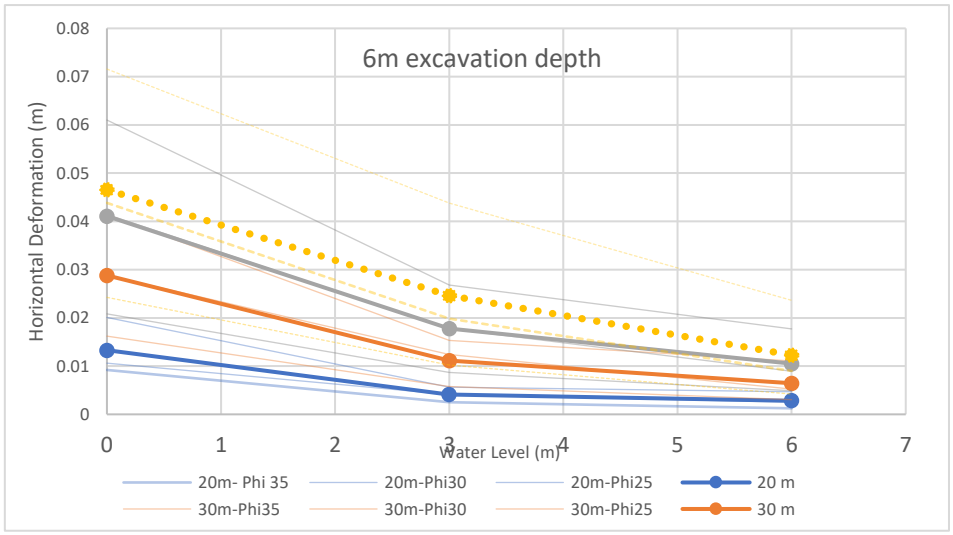

Figure 11.Horizontal deformation of the wall with respect to underground water level in excavation with 6m depth

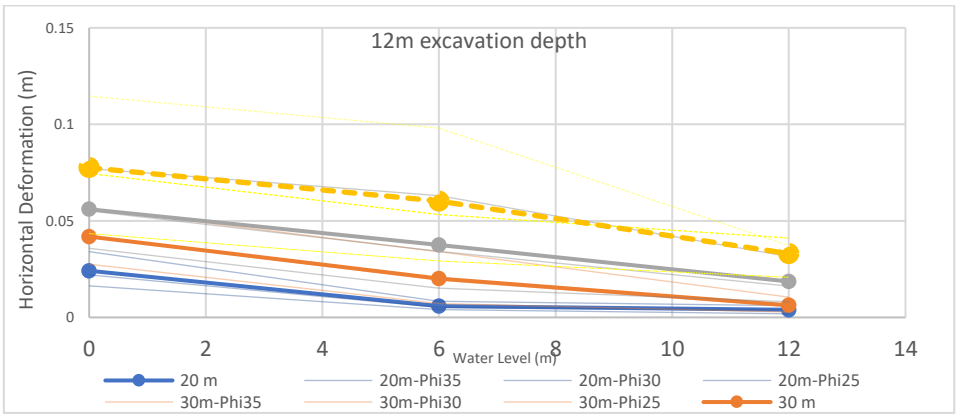

Figure 12. Horizontal deformation of the wall with respect to underground water level in excavation with 12m depth

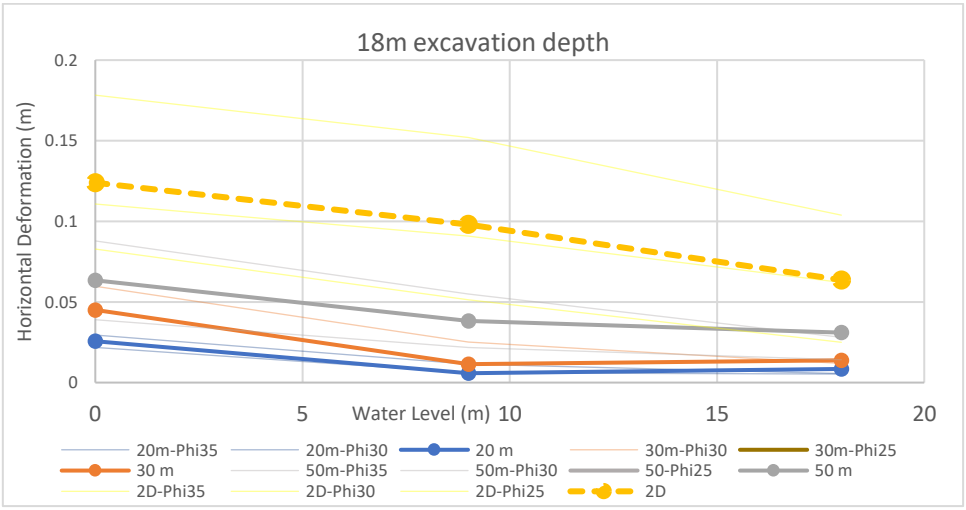

Figure 13. Horizontal deformation of the wall with respect to underground water level in excavation with 18m depth

The distribution of bending moments along the wall, mirrors the deformation trend as seen in Figure 14 to Figure 16. With water table at the ground surface, the hydrostatic pressure and reduced effective stress produces significant lateral demand and larger bending moments,

but as the groundwater is drawn down, the reduction in hydrostatic pressure yields smaller peak moments. The addition of anchors changes this picture by providing discrete reaction points which transform the structural system from a single cantilever into a multi supported beam. Anchors redistribute the lateral load into the ground, thereby reduces the maximum bending moment of the wall and lowering the curvature and deflection (classical beam-theory behavior).

The influence of 3D geometry is also evident; narrower excavations benefit from three-dimensional corner restraint that suppresses displacements and bending demands with respect to plane-strain simulation, whereas as the excavated width increases the 3D results converge toward the 2D plane-strain solution. This corner effect and the divergence between 2D and 3D models are well documented in experimental and numerical studies of Liao et al and Moormanni [12], [24] confirm that fully 3D analyses can produce lower (and more realistic) structural demands than routine 2D approximations, with important implications for optimized, less conservative, and potentially less costly designs.

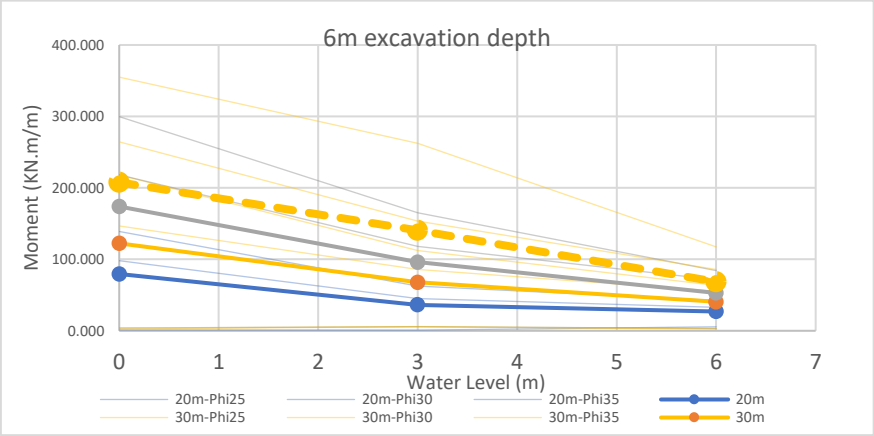

Figure 14. Maximum bending moment distribution in 6 m excavation depth under varying groundwater levels

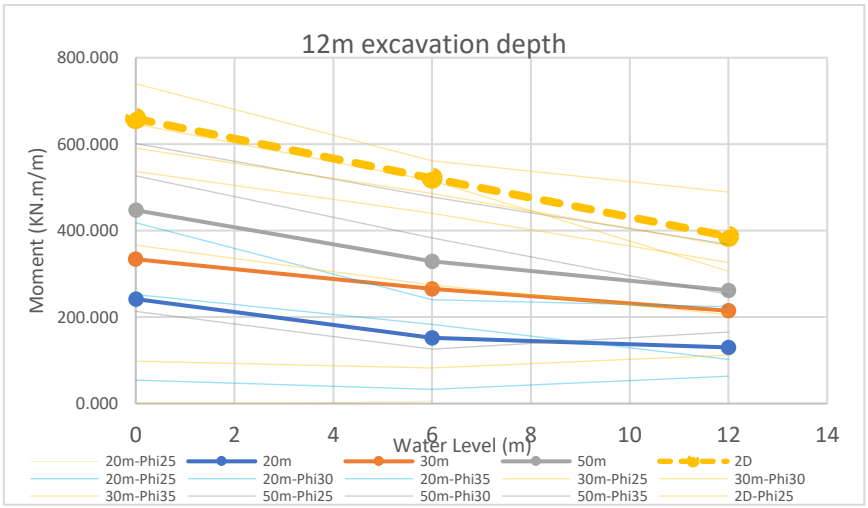

Figure 15. Maximum bending moment distribution in 12 m excavation depth under varying groundwater levels

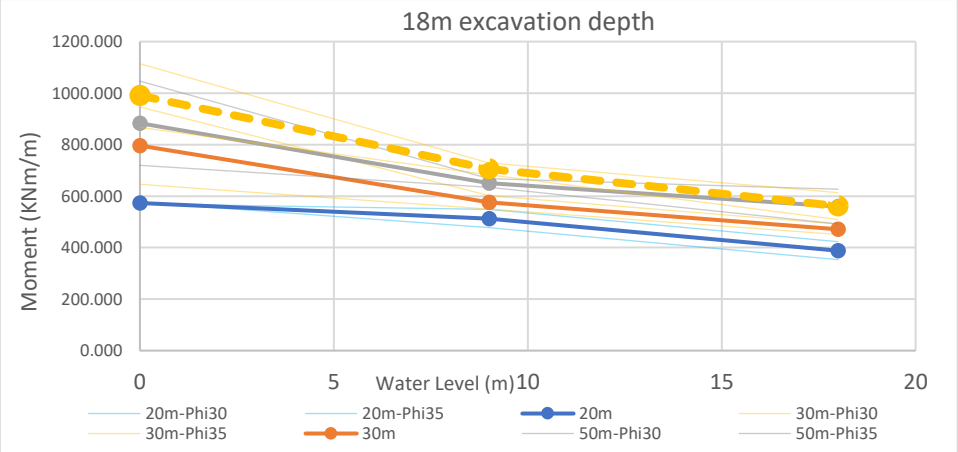

Figure 16. Maximum bending moment distribution in 18 m excavation depth under varying groundwater levels

The results of this study demonstrate a substantial reduction in both horizontal wall deformation and maximum bending moment when using three-dimensional analyses compared to conventional two-dimensional plane-strain simulations. This reduction correlates with, additional restraint mobilized at excavation corners, which cannot be captured in 2D analyses. Table 5 captures the reduction of 3D predictions with respect to 2D analyses for the three excavation depths considered. For a 20 m wide excavation, 3D analyses reduced wall deformations by approximately 61–69% and bending moments by 33–62%, highlighting the strong influence of corner effects in narrow geometries. For a width of 30 m, reductions remained significant, while for the width of 50 m, the reductions were smaller but still non-negligible (9–38% in deformation and 8–17% in moment)

Table 5. Percentage of reduction in results of deformation and moment in 3D analysis with respect to 2D plain strain (%)

EXCAVATION WIDTH (m)		EXCAVATION DEPTH (m)		
		6	12	18
20	Deformation	62%	61%	69%
	Moment	62%	57%	33%
30	Deformation	36%	47%	44%
	Moment	44%	40%	23%
50	Deformation	9%	33%	38%
	Moment	17%	14%	8%

These results emphasize the fact that conventional 2D plane-strain models tend to overpredict structural demand. Therefore, adopting 3D numerical analyses in design practice could yields more realistic predictions of wall performance, supporting more cost-effective and yet safe, excavation support design.

4. Conclusion

This study investigated the optimum design of secant piles - anchorage excavation support systems in cohesionless sands. By integrating LEM optimization with finite element analyses, it was noted that:

1. Groundwater conditions are the most critical parameter influencing anchor demand; as the water table rises, the normalized anchor consumption ratio (β) increases sharply. The considered support system showed stability across soil types under investigation, while secant piles resisting shear at depth and anchors effectively limiting wall displacements and redistributing bending moment.
2. 2D analyses tend to overestimate wall deformations and bending moments. Whereas, 3D simulations accounted for excavation width and corner effects, leads to reductions of up to 62% in wall deformation and moment. This emphasizes that design based solely on 2D models may be uneconomical. Hence adopting 3D simulations enables more accurate and cost-efficient support designs.
3. The proposed β ratio provides a useful indicator for assessing efficiency of a design and avoiding over budgeting excavation phase of the construction.

In summary, through these findings, authors suggest the use of 3D finite element modeling in practice to achieve both safety and economic optimization in excavation support design.

5. Acknowledgments

During the preparation of this work, the authors used *OpenAI* in order to check spelling, grammar and improve the readability of the manuscript. After using this tool, the authors reviewed and edited the content as needed and take full responsibility for the content of the publication.

References

[1] P. Jamsawang, P. Voottipruex, P. Jongpradist, and S. Likitlersuang, "Field and three-dimensional finite element investigations of the failure cause and rehabilitation of a composite soil-cement retaining wall," *Eng Fail Anal*, vol. 127, Sep. 2021, doi: 10.1016/j.engfailanal.2021.105532.

[2] Y. P. Dong, H. J. Burd, and G. T. Houlsby, "Finite element analysis of a deep excavation case history," Nov. 2017.

[3] A. Satyanaga *et al.*, "Building Information Modelling for Application in Geotechnical Engineering," Jun. 01, 2023, *MDPI*. doi: 10.3390/infrastructures8060103.

[4] K. Marek, B. Wiesław, S. G. Anna, W. Zbigniew, and G. Sławomir, "Experimental Validation of Deflections of Temporary Excavation Support Plates with the Use of 3D Modelling," *Materials*, vol. 15, no. 14, Jul. 2022, doi: 10.3390/ma15144856.

[5] R. Ignat, S. Baker, S. Larsson, and S. Liedberg, "Two- and three-dimensional analyses of excavation support with rows of dry deep mixing columns," *Comput Geotech*, vol. 66, pp. 16–30, May 2015, doi: 10.1016/j.compgeo.2015.01.011.

[6] W. Liu, J. Mao, H. Zhao, and G. Shao, "Experimental Study on Double Row Micropiles and Anchors Composite Retaining Structure in Deep Fill Site," *Advances in Civil Engineering*, vol. 2022, 2022, doi: 10.1155/2022/5662220.

[7] T. Su, Y. Zhou, Z. Wang, and S. Ye, “Large Scale Model Test Study of Foundation Pit Supported by Pile Anchors,” *Applied Sciences (Switzerland)*, vol. 12, no. 19, Oct. 2022, doi: 10.3390/app12199792.

[8] R. Kayen *et al.*, “Geoengineering and seismological aspects of the Niigata-Ken Chuetsu-Oki earthquake of 16 July 2007,” *Earthquake Spectra*, vol. 25, no. 4, pp. 777–802, 2009, doi: 10.1193/1.3240397.

[9] M. Crisp, M. Macdonald Group, and O. Davies, “A tool for soil nail wall design optimisation using Slide2 and Python,” Nov. 2022. [Online]. Available: https://www.researchgate.net/publication/378336998

[10] C. R. Bettini, O. C. Longo, L. F. Alcoforado, and A. C. G. Maia, “Method for Estimating of Construction Cost of a Building Based on Previous Experiences,” *Open Journal of Civil Engineering*, vol. 06, no. 05, pp. 749–763, 2016, doi: 10.4236/ojce.2016.65060.

[11] F. Antoniou, G. Aretoulis, D. Giannoulakis, and D. Konstantinidis, “Cost and Material Quantities Prediction Models for the Construction of Underground Metro Stations,” *Buildings*, vol. 13, no. 2, Feb. 2023, doi: 10.3390/buildings13020382.

[12] S.-M. Liao, W.-L. Li, Y.-Y. Fan, X. Sun, and Z.-H. Shi, “Model Test on Lateral Loading Performance of Secant Pile Walls,” 2014, doi: 10.1061/(ASCE)CF.1943.

[13] A. R. Jumikis, *Foundation Engineering*. Englewood Cliffs, NJ: Prentice-Hall, 1971.

[14] R. B. Peck, W. E. Hanson, and T. H. Thornburn, *Foundation Engineering*, 2nd ed. New York: John Wiley & Sons, 1974.

[15] G. P. Tschebotarioff, *Foundations, Retaining and Earth Structures*, 2nd ed. New York: McGraw-Hill, 1973.

[16] I. of C. E. (Great B. Andrew Lees, *Geotechnical finite element analysis : a practical guide*. ICE Publishing, London, 2016, 2016.

[17] M. Maleki, H. Mohammad Nezhad, and S. M. Mir Mohammad Hosseini, “A numerical study of site effect and dynamic response of staged excavation supported by soil nail walls,” *Sci Rep*, vol. 15, no. 1, Dec. 2025, doi: 10.1038/s41598-025-05510-2.

[18] P. J. Sabatini, D. G. Pass, and R. C. Bachus, “GEOTECHNICAL ENGINEERING CIRCULAR NO. 4 Ground Anchors and Anchored Systems (FHWA),” 1999.

[19] Seequent GeoStudio, “Slope Stability Verification Manual”, Accessed: Sep. 02, 2025. [Online]. Available: https://files.seequent.com/GeoStudio/Manuals/Slope%20Stability%20Verification%20Manual.pdf

[20] P. K. Kaiser and K. J. Hewitt, “The effect of groundwater flow on the stability and design of retained excavations.,” *Canadian Geotechnical Journal*, vol. 19, no. 2, pp. 139–153, 1982, doi: 10.1139/t82-016.

[21] “PLAXIS Scientific Manual 2D,” Mar. 2024.

[22] M. Sadek and I. Shahrour, “A three dimensional embedded beam element for reinforced geomaterials,” *Int J Numer Anal Methods Geomech*, vol. 28, no. 9, pp. 931–946, Aug. 2004, doi: 10.1002/nag.357.

[23] B. M. Youssef A Hashash, A. Member, A. J. Whittle, and Z. Member, “GROUND MOVEMENT PREDICTION FOR DEEP EXCAVATIONS IN SOFT CLAY.”

[24] C. Moormanni, “NII-Electronic Library Service ANALYSIS OF WALL AND GROUND MOVEMENTS DUE TO DEEP EXCAVATIONS IN SOFT SOIL BASED ON A NEW WORLDWIDE DATABASE,” Japanese Geotechnical Society, 2004.

Appendix 1

Following table shows the final design of each 81 model and the results of 2D analysis. Where **H** is the height (depth) of the excavation, **ϕ** is the internal friction angle of the soil, H_w is the water level, **q** is the surcharge load, **L** is the total length of anchorage, L_b is the bond lengt, h_a is the vertical distance between two anchors and **Sa** is the horizontal distance between two anchors, **n** is the total number of rows of anchors, **β** is the anchorage consumption rate, δ_x is the horizontal deformation of the wall, **FS** is the safety factor achieved for the critical slope surface using LEM method. $\frac{\delta x}{H}$ is the ratio between the horizontal displacement and the depth of the excavation.

Modell	H(m)	ϕ	H_w (m)	q	L(m)	L_b(m)	h_a(m)	s_a(m)	n	β $(\frac{1}{m})$	δ_X(m)	FS	$\delta x/_H$
1	6	25	0	30	11	7	1.50	1.5	4	4.889	0.059	1.384	0.010
2	6	25	0	60	11	7	1.5	1.5	4	4.889	0.068	1.424	0.011
3	6	25	0	90	11	7	1.5	1.5	4	4.889	0.088	1.373	0.015
4	6	25	3	30	11	7	3	2	2	1.833	0.033	1.378	0.005
5	6	25	3	60	11	7	3	2	2	1.833	0.056	1.466	0.009
6	6	25	3	90	11	7	2	2	3	2.750	0.042	1.408	0.007
7	6	25	6	30	11	7	3	2	2	1.833	0.010	1.68	0.002
8	6	25	6	60	11	7	3	2	2	1.833	0.036	1.483	0.006
9	6	25	6	90	11	7	3	2	2	1.833	0.025	1.544	0.004
10	6	30	0	30	12	6	3	2	2	2.000	0.035	1.525	0.006
11	6	30	0	60	12	6	2	2	3	3.000	0.036	1.408	0.006
12	6	30	0	90	15	8	1	2	5	6.250	0.060	1.479	0.010
13	6	30	3	30	11	5	----	2	1	0.917	0.022	1.562	0.004
14	6	30	3	60	12	6	----	2	1	1.000	0.019	1.476	0.003
15	6	30	3	90	12	6	3	2	2	2.000	0.018	1.571	0.003
16	6	30	6	30	10	5	----	2	1	0.833	0.007	1.457	0.001
17	6	3	6	60	12	6	----	2	1	1.000	0.011	1.397	0.002
18	6	3	6	90	12	6	3	2	2	2.000	0.009	1.549	0.001
19	6	35	0	30	9	5	3	2	2	1.500	0.029	1.603	0.005
20	6	35	0	60	9	5	3	2	2	1.500	0.021	1.484	0.003
21	6	35	0	90	9	5	3	2	2	1.500	0.023	1.408	0.004
22	6	35	3	30	9	5	----	2	1	0.750	0.008	1.49	0.001
23	6	35	3	60	9	5	----	2	1	0.750	0.011	1.596	0.002
24	6	35	3	90	9	5	3	2	2	1.500	0.012	1.692	0.002
25	6	35	6	30	9	5	----	2	1	0.750	0.002	1.405	0.000
26	6	35	6	60	9	5	----	2	1	0.750	0.006	1.482	0.001
27	6	35	6	90	9	5	----	2	1	0.750	0.005	1.48	0.001
28	12	25	0	30	25	13	1.5	1	8	16.667	0.091	1.515	0.008
29	12	25	0	60	25	13	1	1	8	16.667	0.110	1.574	0.009
30	12	25	0	90	25	13	1	1	11	22.917	0.143	1.523	0.012
31	12	25	6	30	21	10	2	2	6	5.250	0.076	1.74	0.006
32	12	25	6	60	22	13	2	2	6	5.500	0.091	1.328	0.008

33	12	25	6	90	24	13	2	2	6	6.000	0.127	1.557	0.011
34	12	25	12	30	18	9	2	2	6	4.500	0.025	1.633	0.002
35	12	25	12	60	20	12	2	2	6	5.000	0.037	1.359	0.003
36	12	25	12	90	24	13	2	2	6	6.000	0.050	1.625	0.004
37	12	3	0	30	20	9	1	1.5	11	12.222	0.074	1.439	0.006
38	12	3	0	60	22	9	1.5	1	8	14.667	0.071	1.771	0.006
39	12	3	0	90	17	8	1	1.5	11	10.389	0.079	1.43	0.007
40	12	30	6	30	17	8	2	2	5	3.542	0.041	1.708	0.003
41	12	30	6	60	16	8	2	2	5	3.333	0.054	1.376	0.004
42	12	30	6	90	18	8	2	2	5	3.750	0.065	1.339	0.005
43	12	30	12	30	12	5	2	2	4	2.000	0.032	1.335	0.003
44	12	30	12	60	14	8	2	2	5	2.917	0.045	1.783	0.004
45	12	30	12	90	18	8	2	2	5	3.750	0.046	1.384	0.004
46	12	35	0	30	18	7	2	1.5	5	5.000	0.033	1.855	0.003
47	12	35	0	60	18	7	2	1.5	5	5.000	0.040	1.741	0.003
48	12	35	0	90	18	7	2	1.5	5	5.000	0.057	1.363	0.005
49	12	35	6	30	14	7	2	2	3	1.750	0.022	1.382	0.002
50	12	35	6	60	16	7	2	2	5	3.333	0.022	1.303	0.002
51	12	35	6	90	15	7	2	2	5	3.125	0.044	1.408	0.004
52	12	35	12	30	11	6	3	2	3	1.375	0.021	1.312	0.002
53	12	35	12	60	15	7	2	2	5	3.125	0.013	1.464	0.001
54	12	35	12	90	15	7	2	2	5	3.125	0.029	1.469	0.002
55	18	25	0	30	25	14	1	1	17	23.611	0.104	1.317	0.006
56	18	25	0	60	25	14	1	1	17	23.611	0.149	1.313	0.008
57	18	25	0	90	25	15	1	1	17	23.611	0.281	1.29	0.016
58	18	25	9	30	25	13	1	1	17	23.611	0.100	1.335	0.006
59	18	25	9	60	25	13	1	1	17	23.611	0.105	1.495	0.006
60	18	25	9	90	25	14	1	1	12	23.611	0.251	1.461	0.014
61	18	25	18	30	25	14	2	1.5	9	8.333	0.070	1.782	0.004
62	18	25	18	60	23	9	2	1	8	10.222	0.096	1.327	0.005

Model	H(m)	ϕ	H_W (m)	q	L(m)	L_b(m)	h_a(m)	s_a(m)	n	L/A $(\frac{m}{m2})$	δ_x(m)	FS	$\delta x/_H$
63	18	25	18	90	21	11	1.5	1.5	11	8.556	0.145	1.339	0.008
64	18	30	0	30	24	9	1.5	1.5	11	9.778	0.091	1.585	0.005
65	18	30	0	60	25	8	2	1	17	23.611	0.117	1.3	0.007
66	18	30	0	90	25	8	1	1	17	23.611	0.124	1.352	0.007
67	18	30	9	30	22	9	2	1.5	8	6.519	0.082	1.334	0.005
68	18	30	9	60	22	8	2	1.5	9	7.333	0.075	1.466	0.004
69	18	30	9	90	25	9	2	1	9	12.500	0.115	1.368	0.006
70	18	30	18	30	22	9	2	1.5	9	7.333	0.025	1.523	0.001
71	18	30	18	60	21	8	2	1.5	8	6.222	0.067	1.639	0.004
72	18	30	18	90	20	8	2	1	8	8.889	0.094	1.316	0.005
73	18	35	0	30	25	8	1.5	1	11	15.278	0.038	1.605	0.002
74	18	35	0	60	25	7	1.5	1.5	11	10.185	0.102	1.42	0.006
75	18	35	0	90	25	7	1.5	1.5	11	10.185	0.109	1.334	0.006
76	18	35	9	30	23	8	2	2	8	5.111	0.030	1.415	0.002
77	18	35	9	60	25	8	2	1.5	8	7.407	0.042	1.478	0.002
78	18	35	9	90	18	6	2	1.5	8	5.333	0.083	1.607	0.005
79	18	35	18	30	22	7	2	2	8	4.889	0.028	1.413	0.002
80	18	35	18	60	25	8	2	1.5	8	7.407	0.015	1.661	0.001
81	18	35	18	90	17	6	2	1.5	8	5.037	0.032	1.714	0.002

Appendix 2

The following table summarize the values of horizontal deformation **δ** and bending moment **M** in 3D (20, 30 and 50 m width) and 2D finite element analysis.

Model	H	ϕ	H_w	q (kN/m2)	δ_{20}	δ_{30}	δ_{50}	δ_{2d}	M_{20}	M_{30}	M_{50}	M_{2d}
1	6	25	0	30	0.025	0.032	0.056	0.059	168.51	303.75	534.88	425.29
2	6	25	0	60	0.016	0.035	0.059	0.068	209	519.1	601.75	489.4
3	6	25	0	90	0.019	0.057	0.068	0.088	160.51	249.65	439.13	517.16
4	6	25	3	30	0.004	0.012	0.024	0.033	58	129.77	479.14	334.04
5	6	25	3	60	0.006	0.016	0.030	0.056	44.63	784.2	393.85	373.14
6	6	25	3	90	0.007	0.018	0.026	0.042	74.45	255.37	340.98	403.96
7	6	25	6	30	0.002	0.008	0.012	0.010	180.6	213.2	268.41	285.83
8	6	25	6	60	0.005	0.010	0.017	0.036	186.1	267.23	272.05	319.1
9	6	25	6	90	0.006	0.015	0.024	0.025	265.37	325.55	394.89	363.49
10	6	30	0	30	0.006	0.026	0.033	0.035	121.300	184.900	283.200	346.38
11	6	30	0	60	0.007	0.028	0.034	0.036	142.500	293.800	372.400	395.3
12	6	30	0	90	0.019	0.032	0.057	0.060	153.200	175.600	243.500	323.33
13	6	30	3	30	0.003	0.010	0.020	0.022	59.320	120.600	173.300	299.77
14	6	30	3	60	0.005	0.015	0.017	0.019	63.340	120.600	180.300	220.49
15	6	30	3	90	0.005	0.012	0.016	0.018	64.770	96.300	142.500	267.12
16	6	30	6	30	0.002	0.006	0.007	0.007	41.190	69.660	83.940	110.3
17	6	30	6	60	0.003	0.004	0.011	0.011	45.050	70.190	110.500	152.6
18	6	30	6	90	0.003	0.005	0.009	0.009	41.190	50.600	58.300	89.3
19	6	35	0	30	0.004	0.014	0.023	0.029	91.800	109.800	201.000	224.439
20	6	35	0	60	0.006	0.015	0.019	0.021	97.640	146.700	200.000	270

Model	H	ϕ	H_w	q (kN/m2)	δ_{20}	δ_{30}	δ_{50}	δ_{2d}	M_{20}	M_{30}	M_{50}	M_{2d}
21	6	35	0	90	0.018	0.019	0.020	0.023	104.900	183.600	253.800	298.867
22	6	35	3	30	0.001	0.004	0.008	0.008	42.240	87.200	122.300	150.3
23	6	35	3	60	0.003	0.008	0.009	0.011	46.650	86.750	112.400	150.3
24	6	35	3	90	0.003	0.005	0.009	0.012	46.240	83.240	119.100	160.3
25	6	35	6	30	0.000	0.002	0.003	0.002	31.290	56.060	68.110	75.3
26	6	35	6	60	0.002	0.004	0.006	0.006	32.190	61.440	71.280	103.6
27	6	35	6	90	0.002	0.003	0.005	0.005	35.110	48.580	74.640	78.6
28	12	25	0	30	0.039	0.067	0.079	0.091	45.600	90.100	180.300	473.88
29	12	25	0	60	0.020	0.036	0.063	0.110	55.200	92.500	199.000	824.71
30	12	25	0	90	0.043	0.066	0.089	0.143	63.200	111.200	260.400	473.202
31	12	25	6	30	0.003	0.030	0.036	0.076	25.400	88.970	133.800	485.58
32	12	25	6	60	0.008	0.026	0.058	0.091	35.060	81.650	125.600	506.292
33	12	25	6	90	0.014	0.046	0.095	0.127	38.140	76.490	118.400	466.211
34	12	25	12	30	0.004	0.008	0.018	0.025	25.720	57.480	88.960	386.84
35	12	25	12	60	0.006	0.008	0.029	0.037	17.370	44.920	79.270	369.491
36	12	25	12	90	0.008	0.015	0.048	0.050	147.000	234.100	326.900	337.46
37	12	30	0	30	0.017	0.051	0.062	0.074	326.300	487.200	554.200	665.079
38	12	30	0	60	0.019	0.031	0.042	0.071	406.400	502.000	598.200	731.98
39	12	30	0	90	0.031	0.042	0.061	0.079	521.800	621.200	652.000	821.56
40	12	30	6	30	0.004	0.014	0.024	0.041	238.700	421.900	480.100	520.3

Model	H	ϕ	H_w	q (kN/m2)	δ_{20}	δ_{30}	δ_{50}	δ_{2d}	M_{20}	M_{30}	M_{50}	M_{2d}
41	12	30	6	60	0.006	0.014	0.035	0.054	242.400	448.500	478.900	582.071
42	12	30	6	90	0.006	0.030	0.044	0.065	239.100	448.700	474.200	582.706
43	12	30	12	30	0.004	0.006	0.015	0.032	183.500	293.600	367.100	492.55
44	12	30	12	60	0.005	0.005	0.020	0.045	218.100	353.000	386.900	495.16
45	12	30	12	90	0.002	0.005	0.014	0.046	270.500	332.300	350.300	479.91
46	12	35	0	30	0.005	0.023	0.031	0.033	324.600	496.500	720.600	850.204
47	12	35	0	60	0.018	0.023	0.036	0.040	151.200	210.500	378.700	541.96
48	12	35	0	90	0.026	0.036	0.040	0.057	280.300	392.200	480.300	546.134
49	12	35	6	30	0.003	0.006	0.015	0.022	201.500	254.200	360.300	565.02
50	12	35	6	60	0.005	0.009	0.017	0.022	147.900	195.300	332.700	463.35
51	12	35	6	90	0.004	0.006	0.013	0.044	200.300	372.900	455.000	517.55
52	12	35	12	30	0.001	0.002	0.012	0.021	93.250	208.900	211.900	299.58
53	12	35	12	60	0.003	0.004	0.009	0.013	105.400	130.200	251.300	305.062
54	12	35	12	90	0.001	0.002	0.003	0.029	107.800	278.300	293.400	313.98
55	18	25	0	30	**	**	**	0.104	**	**	**	3008.56
56	18	25	0	60	**	**	**	0.149	**	**	**	1970.47
57	18	25	0	90	**	**	**	0.281	**	**	**	2322.88
58	18	25	9	30	**	**	**	0.100	**	**	**	1608.99
59	18	25	9	60	**	**	**	0.105	**	**	**	1248.91
60	18	25	9	90	**	**	**	0.251	**	**	**	1724.1

Model	H	ϕ	H_w	q (kN/m2)	δ_{20}	δ_{30}	δ_{50}	δ_{2d}	M_{20}	M_{30}	M_{50}	M_{2d}
61	18	25	18	30	0.011	0.017	0.037	0.070	287.500	527.000	774.500	810.78
62	18	25	18	60	0.020	0.028	0.081	0.096	538.300	851.000	1042.000	1159.96
63	18	25	18	90	0.012	0.021	0.034	0.145	416.600	770.800	980.100	1292.531
64	18	30	0	30	0.028	0.081	0.088	0.091	541.400	923.900	989.600	1274.91
65	18	30	0	60	0.028	0.041	0.062	0.117	579.600	942.600	1001.300	1046.29
66	18	30	0	90	0.033	0.057	0.114	0.124	588.000	972.400	1149.000	1020.95
67	18	30	9	30	0.008	0.019	0.062	0.082	592.800	623.600	727.900	738.701
68	18	30	9	60	0.017	0.025	0.034	0.075	583.000	620.500	681.700	750.46
69	18	30	9	90	0.009	0.032	0.069	0.115	470.500	562.700	593.540	696.074
70	18	30	18	30	0.005	0.014	0.020	0.025	453.000	498.300	533.220	564.93
71	18	30	18	60	0.008	0.017	0.033	0.067	555.500	617.000	836.600	715.6
72	18	30	18	90	0.003	0.005	0.031	0.094	260.200	358.700	510.510	560.3
73	18	35	0	30	0.010	0.026	0.037	0.038	498.800	573.200	635.200	890.8
74	18	35	0	60	0.021	0.025	0.038	0.102	670.900	681.200	793.100	848.35
75	18	35	0	90	0.034	0.040	0.043	0.109	560.300	683.500	730.600	861.47
76	18	35	9	30	0.005	0.009	0.027	0.030	397.500	503.200	600.300	670.6
77	18	35	9	60	0.009	0.011	0.024	0.042	487.800	510.300	579.300	626.767
78	18	35	9	90	0.004	0.007	0.014	0.083	545.800	635.400	722.300	750.3
79	18	35	18	30	0.005	0.009	0.018	0.028	191.600	373.900	448.500	459.78
80	18	35	18	60	0.007	0.010	0.014	0.015	425.800	451.200	470.200	498.56
81	18	35	18	90	0.004	0.002	0.011	0.032	442.300	528.000	557.400	568.82